Spectrochimica Acta Part A: Molecular and Biomolecular Spectroscopy 205 (2018) 132–138

Contents lists available at ScienceDirect

Spectrochimica Acta Part A: Molecular and Biomolecular Spectroscopy

journal homepage: www.elsevier.com/locate/saa

Local-dependency of morphological and optical properties between breast cancer cell lines

Seung Ho Lee [a], Ok-Kyun Kim [a], Sanghwa Lee [b,c,*,1], Jun Ki Kim [c,d,**,1]

[a] Department of Biochemistry & Molecular Biology, College of Medicine, Kyung Hee University, 23, Kyungheedae-ro, Dongdaemun-gu, Seoul 02447, Republic of Korea
[b] Department of Biomedical Engineering, College of Medicine, Kyung Hee University, 23, Kyungheedae-ro, Dongdaemun-gu, Seoul 02447, Republic of Korea
[c] Biomedical Engineering Research Center, Asan Medical Center, 88, Olympic-ro 43-gil, Songpa-gu, Seoul 138-736, Republic of Korea
[d] Department of Convergence Medicine, University of Ulsan College of Medicine, 88, Olympic-ro 43-gil, Songpa-gu, Seoul 138-736, Republic of Korea

ARTICLE INFO

Article history:
Received 31 January 2018
Received in revised form 2 July 2018
Accepted 8 July 2018
Available online 09 July 2018

Keywords:
Breast cancer cells
Raman spectroscopy
Atomic force microscopy (AFM)
Optical microscopy
Principal component analysis (PCA)

ABSTRACT

Breast cancer is the most malignant type of cancer in women and is a global health problem, with mortality by metastasis being the main factor among others. Currently, detection and diagnosis of breast cancer is achieved through a variety of procedures, such as clinical examination, medical imaging, biopsy, and histopathological analysis. In contrast, spectroscopic analysis has a variety of advantages such as being noninvasive, not destroying biological materials, and not requiring additional histological analysis. In this study, various approaches using Raman spectroscopy, atomic force microscopy (AFM), and optical microscopy were used together to differentiate between and characterize normal breast cell lines (MCF-10A) and breast cancer cell lines (MDA-MB-231, MDA-MB-453). Raman spectra of normal breast cell and breast cancer cell lines confirmed visual differences in the concentrations of various compounds. These spectra were also analyzed using principle component analysis (PCA), and the PCA results showed reliable separation of the three cell lines and the cancer cell lines (MDA-MB-231, MDA-MB-453). With these results, optically synchronizing the AFM morphology, the Raman spectroscopy, and the visible RGB optical transmission intensity provided contrasts for not only conformational differences but also intracellular variation between the normal and cancer cell lines. We observed the inherent characteristic that there is no local difference in cancer cells regardless of morphology in a wide range of optical properties such as absorption, scattering and inelastic scattering.

© 2018 Elsevier B.V. All rights reserved.

1. Introduction

Currently, breast cancer is a global problem and the most malignant cancer in women, with mortality arising from metastasis and other factors [1]. Approximately 1.4 million women worldwide experienced breast cancer in 2008, and breast cancer also commonly migrates to other sites [2]. Numerous studies are ongoing, investigating the diagnosis and treatment of breast cancer [3, 4]. The detection and diagnosis of breast cancer is currently achieved through various procedures, such as clinical examination, medical imaging (mammography, computed tomography [CT], magnetic resonance imaging [MRI], ultrasound, etc.), biopsy, histopathological analysis, and surgery. In particular, histopathological analyses including immunohistostaining can reliably detect changes at the molecular level such as in structure and concentration, but have disadvantages such as being invasive, costly, and time consuming [5]. In this regard, vibrational spectroscopic diagnosis offers several advantages, namely being noninvasive, preserving cell tissues, and not requiring any additional labeling [6–10]. Vibrational spectroscopic techniques such as infrared (IR) and Raman spectroscopy have been widely applied in examining chemical and molecular changes in biological samples [11–13]. This approach is able to fingerprint biomolecule composition without the need for additional labeling or purification [14–16].

Recently, Raman spectroscopy has been re-evaluated as a tool for examination of biological samples from the breast, lung, stomach and other organs [17–22]. Raman spectroscopy is based on inelastic scattering of photons that are incident on the sample. When a single-energy laser beam is injected into the sample, the incident energy is transferred by molecular vibrations to stokes-shifted photons that are emitted from the sample as a spectrum. Because the initial energy is diverted by various molecular vibrational modes, the individual peaks of the spectrum contain structural and conformational information. Therefore, Raman is an excellent tool for identifying as cancerous tissue and cells [23–28]. However, Raman mainly provides chemical information but does not provide information on surface morphology and optical properties.

* Correspondence to: S. Lee, Biomedical Engineering Research Center, Asan Medical Center, 88, Olympic-ro 43-gil, Songpa-gu, Seoul 138-736, Republic of Korea.
** Correspondence to: J.K. Kim, Department of Convergence Medicine, University of Ulsan College of Medicine, 88, Olympic-ro 43-gil, Songpa-gu, Seoul 138-736, Republic of Korea.
E-mail addresses: pause19@khu.ac.kr (S. Lee), kim@amc.seoul.kr (J.K. Kim).
[1] These authors contributed equally to this work and are co-corresponding authors.

https://doi.org/10.1016/j.saa.2018.07.024
1386-1425/© 2018 Elsevier B.V. All rights reserved.

Thus, combining modalities for morphological and optical analysis would be highly meaningful.

Atomic force microscopy (AFM) has been widely used in biological studies to examine phenomena such as the cytotoxicity of cellular systems [29] and the mechanical properties of cells and molecules [30, 31]. Furthermore, AFM has been applied to investigate cellular stiffness and Young's modulus, which can in turn differentiate between non-malignant and breast cancer cells [32, 33]. From the AFM results, it is now well-known that cancerous cells are remarkably softer than normal cells.

In the present study, Raman signals were analyzed by localization through synchronization with AFM having high spatial resolution and optical microscopy as shown in Fig. 1. The topography of AFM provides information on local quantitative thicknesses and volumes, revealing the relationships between local Raman spectra and intensities. By introducing local RGB intensity in optical measurements, factors that can be used to distinguish healthy cells from cancer cells were identified. Optical microscopy provided an image of the transmitted light, while the intensity of each pixel of the RGB indicated internal events such as absorption and scattering. AFM revealed that the difference in height within each cell was approximately 1.5 μm. However, inelastic scattering Raman and transmitted light optical microscopy did not identify local variations in cancer cells, unlike in normal cells.

2. Materials and Methods

2.1. Cell Culture

Non-tumorigenic breast epithelial cell line (MCF-10) and two human breast cancer cell lines (MDA-MB-231 and MDA-MB-453) were purchased from the American Type Culture Collection (Manassas, VA, USA) and the Korea Cell Line Bank (Seoul, South Korea). The cell lines were cultured using Dulbecco's modified Eagle's Minimal Essential Medium (DMEM; Life Technologies, Inc., Grand Island, NY, USA) supplemented with 10% fetal bovine serum (FBS; Hyclone Laboratories, Logan, UT, USA) and 1% penicillin-streptomycin solution (Life Technologies, Inc.) in a humidified 5% CO_2 incubator at 37 °C. The human breast epithelial cell lines were cultured using mammary epithelium growth medium (MEGM™ BulletKit™; Lonza Group Ltd., Basel, Switzerland), except for GA-1000 (gentamycin-amphotericin B mix), with the addition of 100 ng/ml cholera toxin from Sigma-Aldrich (St. Louis, MO, USA) in a humidified 5% CO_2 incubator at 37 °C.

2.2. Sample Preparation

All cells were cultured on gold-coated substrates in Petri dishes until they reached 70–80% confluency. After 24 h, phosphate buffered saline (PBS) was removed. Cells were fixed using 4% paraformaldehyde for 20 min at 37 °C and 5% humidity in an incubator and subsequently washed three times in PBS for 10 min each time. Before the Raman measurements, the cells were rinsed with distilled water approximately 10 times to remove the PBS. Before the Raman measurements, the cells were rinsed with distilled water approximately ten times to avoid the PBS component interference.

2.3. Raman Spectroscopy

Raman line maps were measured using a SENTERRA confocal Raman system (Bruker Optics, Billerica, MA, USA). A 785 nm diode laser source with 100 mW power was used for excitation. The light was focused on the cells through a 50×/0.4 NA objective with an approximate spot size of 2.4 μm. Raman lines were mapped through a raster scan at approximately 2.5 μm of step which refers to the distance between laser beam centers. The spectrum of each point was measured twice in the range of 400 to 2500 cm^{-1} with a spectral resolution of 5 cm^{-1} and an integration time of 30 s at room temperature. Before the Raman measurements, the Raman spectrum was calibrated by measuring a silicon sample. Following the Raman measurements, the spectrum was preprocessed by a Savitzky-Golay smoothing filter, the autofluorescence background was removed by a third-order polynomial fitting, and the substrate noise signal was subtracted to make the spectrum better suited for an analysis.

2.4. Atomic Force Microscopy

Topography and surface roughness data were acquired using an atomic force microscope (TT-AFM, AFM workshop) in a nonvibrational mode at room temperature. Both types of cells fixed on a gold coated substrate of approximately 15 nm roughness (RMS value) were mounted on the AFM x-y piezo stage for scanning. A topography area of 50 μm × 50 μm was constructed using 256 scan lines and a scanning rate of 0.2 Hz.

2.5. Synchronization Between Raman and AFM

After the samples were prepared, the rinsed cells were dried and alignment markers were printed on them before the Raman measurements. The individual cells measured by Raman spectroscopy were labeled with distance from the alignment marker and magnitude of the objective lens. To position the cells and rotate substrate, alignment markers on the sample and a cross bar on the AFM optical image were matched prior to approaching and positioning the cantilever. The magnitudes of the AFM topography and the Raman optical image were synchronized by a scale on AFM and Raman.

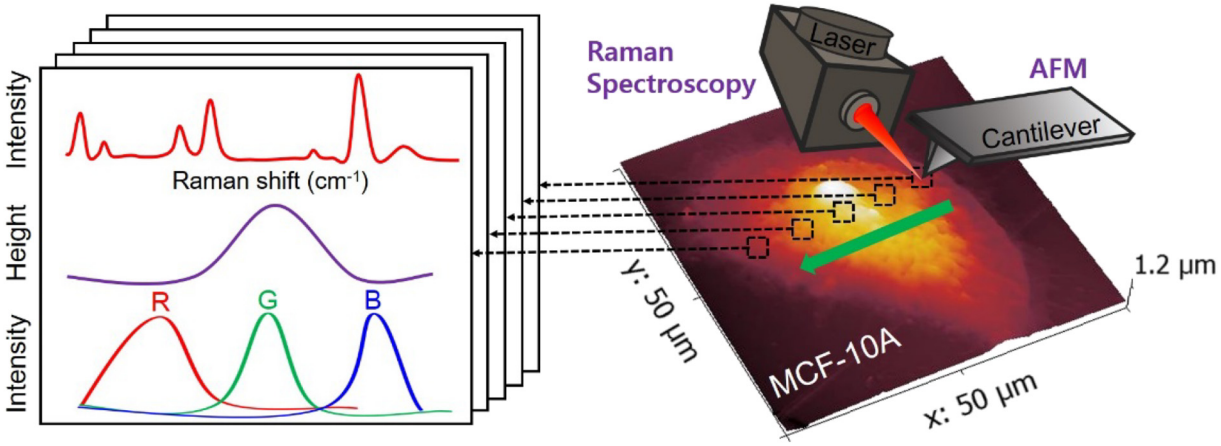

Fig. 1. Schematic diagram showing the examination of healthy and cancer cell lines using various types of spectroscopy.

2.6. Optical Microscopy and RGB Profile

Reflection and transmission optical microimages were observed using an optical microscope (BX51, Olympus) with mercury and halogen white light sources, respectively. A 50× objective lens and a second lens of 2× magnification were combined, along with an extended focal imaging calculation, to reduce chromatic aberration and blurred image edges on the reflected and transmitted images. Snap images were acquired within 1 s, and the resolution of all images was 1360 × 1024 pixels. For measurements of reflection images, white paper was initially mounted as a white calibration target and subsequently optical images and RGB profiles were acquired. For optical transmission imaging, white valence was performed on the bare gold surface.

2.7. Raman Data Analysis

Auto-fluorescence spectra were removed from Raman data using Bruker OPUS 7.0 spectroscopy software. The remaining Raman spectrum reflects the conformational characteristics of the samples in addition to the background noise. Therefore, signal processing including smoothing and baseline correction was necessary for accurate data analysis of each sample. We evaluated the spectral differences between the normal and cancer cell lines using principal component analysis (PCA). PCA is a general multivariate statistical analysis technique that minimizes the number of predictive variables. In this study, PCA was conducted as an attempt to group useful information from the preprocessed Raman spectra and to highlight the differences between MFC-10A, MDA-MB-231 and MDA-MB-453. All analyses were conducted using the XLSTAT 2016 software (Microsoft, Redmond, WA, USA).

3. Results and Discussion

3.1. Raman Spectra of the Breast Cell and Cancer Cell Lines

Three cells were examined by Raman spectroscopy in order to determine the differences between normal cells and cancer cells, and these cells were selected because they play an important role in cancer metastasis. The Raman spectra obtained for the normal cell line (MFC-10A) and the breast cancer cell lines (MDA-MB-231, MDA-MB-453) showed major peaks in phenylalanine, amides I and III, CH_2 deformation, CH_2 wagging/twisting and S—S bonding vibration regions as shown in Fig. 2. Each spectrum was previously smoothed and baseline corrected, and the spectra obtained from each cell line showed visual differences including error bars. The concentrations of amide III, CH_2 deformation vibration, CH_2 wagging/twisting, amide I and so on were different in breast cell lines. The difference in Raman spectra can be distinguished by peak position, relative intensity between peaks and absolute intensity of a particular peak, and these species such as amide III, CH_2 deformation vibration, CH_2 wagging/twisting, amide I were labeled from the peak position. The CH_2 deformation and amide I regions showed similar intensities in two cancer cell lines, but the MDA-MB-231 spectrum had a higher relative amount of CH_2 wagging/twisting. In particular, the Raman spectrum for MDA-MB-231 had higher CH_2 wagging/twisting intensity than other cancer cells, and this difference is greater than the error bars in situations where the intensities of other peaks, such as S—S bonding and CH_2 deformation vibration, are similar. These features seem to indicate the different chemical composition characteristics between the cancer cells and normal cells, which is a factor in the statistical analysis. Moreover, these results may be useful as potential main spectrum markers in the analysis of cancer states.

3.2. AFM and Optical Characteristics of Breast Cancer Cells

AFM topology and transmission optical images are shown in Fig. 3, indicating matched line profiles of height, RGB intensity, and Raman spectroscopy. The individual AFM topologies, shown in the left column of (a) MCF-10A, (b) MDA-MB-231 and (c) MDA-MB-453 had 50 μm × 50 μm scan areas that could cover one or two cells in all cases. Minimum data values were shifted such that the height of each cell varied from zero to 1.5 μm. There were no significant differences in height between or within cell species. Transmission optical images are displayed on the right column corresponding to each AFM topogram. Optical MCF-10A images showed whitish cell boundaries, Newton's ring (rainbow-like contours) and blackhead-like points. Most of the blackheads corresponded to hollows on the AFM topography, but this was not always the case. For the invasive cancer cells MDA-MB-231 and MDA-MB-453, as shown in Fig. 3e and f, transmitted images had blackhead-like points, black spots larger than the blackheads, and cell boundaries which were less clear than those of MCF-10A (Fig. 3d). Even though the blackheads on the optical images were highly distributed around the hollows shown on the morphology images, the black spots were located at the highest peak for each cell. Of note, these spots appear in approximately one out of 10 invasive cancer cells. Thus, it appears that whitish boundaries can be a significant indicator of whether or not a cell is invasive, but two cancer cell lines have barely visible boundaries as shown on the right column in Fig. 3.

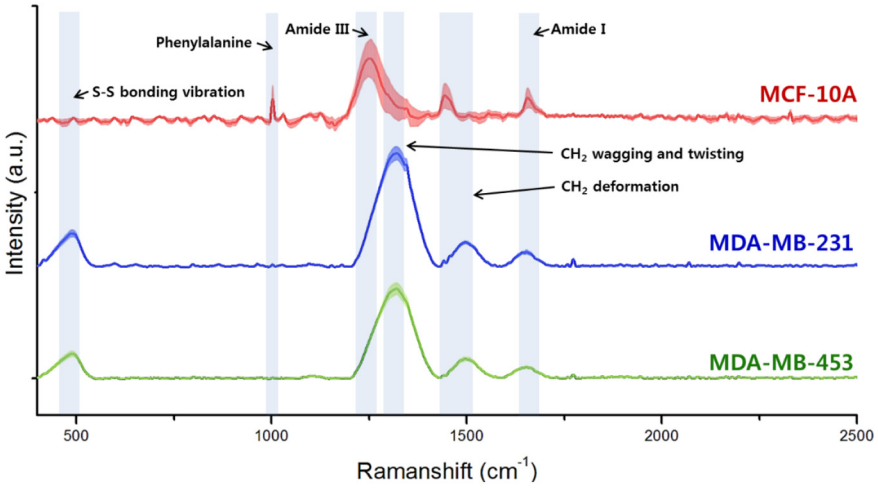

Fig. 2. Mean Raman spectra of the normal breast cell line (a) MCF-10A and the breast cancer cell lines (b) MDA-MB-231 and (c) MDA-MB-453. The error bars for each point are represented by shading around the solid line.

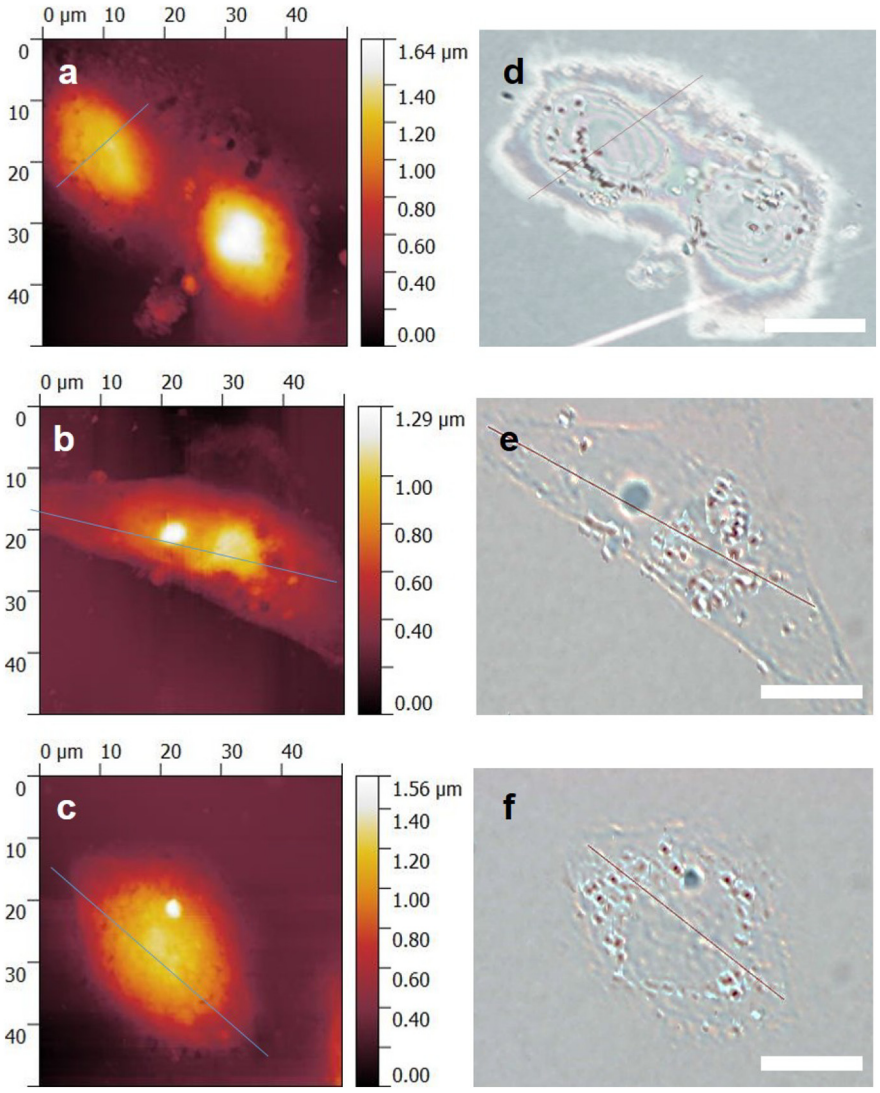

Fig. 3. Matching the topographic and optical images of the three cell lines. AFM images of the noninvasive cells (a) MCF-10A and invasive cell lines (b) MDA-MB-231 and (c) MDA-MB-453 in the first column. Transmission optical images are displayed in the right column to match the measured lines, where the scale bar is 20 µm.

3.3. Synchronization Between Morphological and Optical Properties

To investigate the comparative factors among noninvasive and invasive breast cell lines, line measurements of height, Raman spectroscopy and RGB intensity were performed along the blue lines on the AFM topography and the red line on the optical image, as shown in Fig. 3. In the AFM results, all cross-sectional intensity height profiles were convex, and thus we expected that Raman and RGB intensity would depend on radial differences in cell morphology; thus, each profile covered one cell and was 34 µm long for MCF-10A (as shown in Figs. 4a, d, and e), 47 µm long for MDA-MB-231(as shown in Fig. 4b, e, and h), and 42 µm long for MDA-MB-453 (as shown in Fig. 4c, f, and i). To confirm these findings, we plotted the local differences in Raman signal, phenylalanine, amide I, amide III, and CH_2 deformation, CH_2 wagging/twisting and S—S bonding vibration peaks for individual cell lines synchronized with AFM. With the normal MDF-10A cells, signals of phenylalanine, CH_2 deformation and amide I looked convex, resembling the AFM profile, but the signal for amide III was concave. These findings indicate that the relative ratios of the structural components change along the radial direction within normal cells, but no local dependency was seen in the invasive cell lines. The sequence of downward peak intensity for the invasive cells was maintained with CH_2 wagging/twisting, S—S bonding, CH_2 deformation, amide I, and phenylalanine as shown in Fig. 4e and f.

Furthermore, another notable observation from the present results was the difference in absorption behavior between the normal and cancer cells. The transmitted optical images were acquired after scattering and absorption through the cells, which means that the RGB differences gave information associated with scattering and absorption in the cells. At shorter wavelengths, Rayleigh scattering is more common, and thus the RGB sequence on black spots in MDA-MB-231 was as shown in Fig. 4h, where the range from 18 to 22 µm appeared to indicate scattering. In contrast, the relative ratios of red, green, and blue from MCF-10A in Fig. 4g showed a fringe with no red-green-blue sequence from 14 to 25 µm; the fringe came from the shape of Newton's ring as shown in Fig. 3d, which indicated different material properties between the normal and cancer cells. By introducing standard deviations for RGB intensity, we can compare the intensity quantitatively. The individual deviations in RGB intensity for invasive cell lines were much smaller than those for noninvasive cell lines as shown in Fig. 4g to i. The standard deviations of red, green and blue in MCF-10A were 28.1, 33.0, and 28.8 where the means were 194.0, 209.8, and 215.9, respectively. For the MDA-MB-231 with absorption information at the black spots removed, the standard deviations for RGB intensity were 10.3, 10.1, and

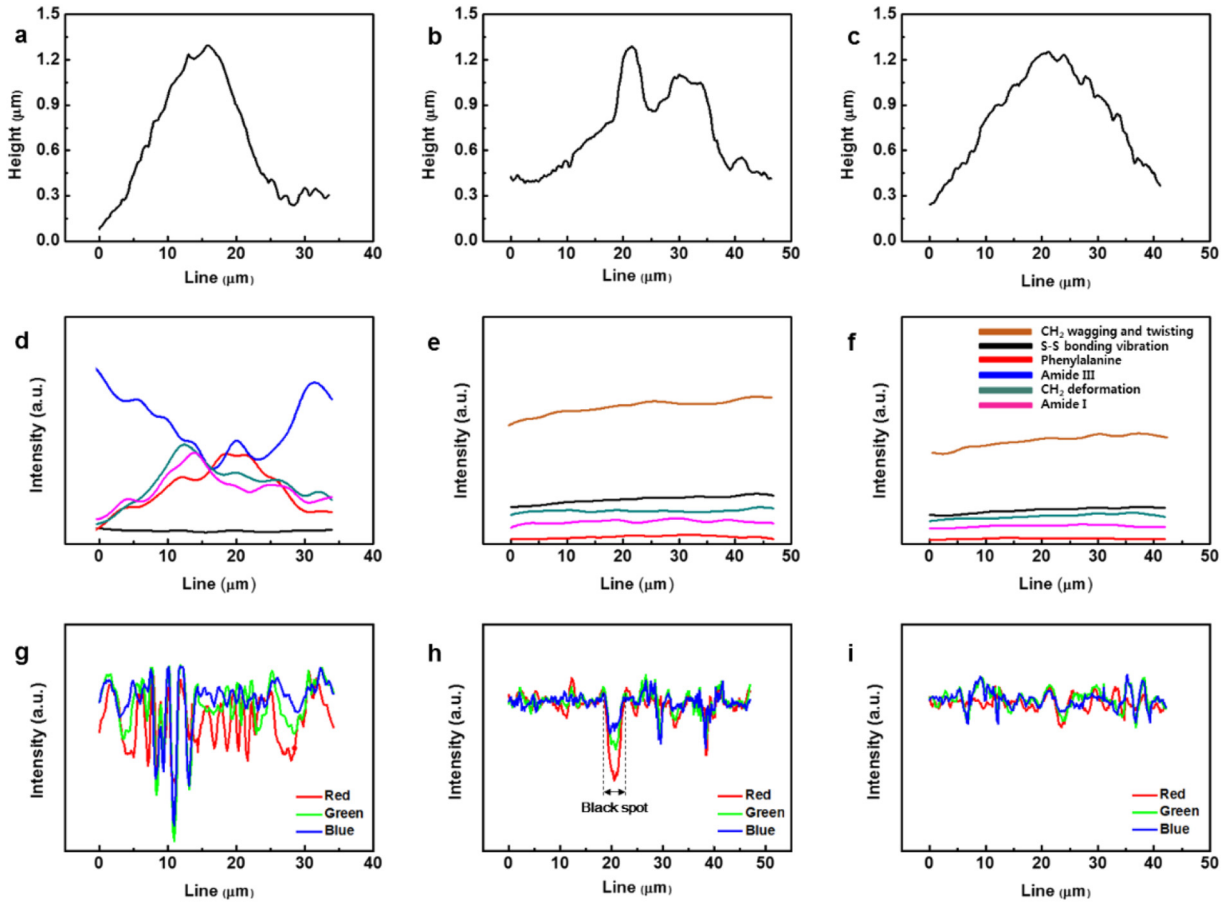

Fig. 4. Comparative results of extracted line morphology (a–c), Raman line scan (d–f), and RGB intensities (g–i) for matching local variations. The first column shows the results for the normal breast cells MCF-10A (a, d and g), and the second and third columns correspond to the breast cancer cell lines MDA-MB-231 (b, e and h) and MDA-MB-453 (c, f and i), respectively. Raman line profiles were plotted for phenylalanine, amide I, amide III, CH_2 deformation, CH_2 wagging/twisting and S—S bonding vibration. The inset in f shows the corresponding colors.

9.2 with RGB means of 213.2, 215.2, and 214.3. In total, the standard deviations of RGB intensity in the noninvasive cell lines were nearly triple those of the invasive cells as summarized in Table 1.

3.4. Principle Component Analysis (PCA)

From the PCA of the spectrum obtained from the cell line, it became possible to further distinguish between three cell lines, and it became possible to distinguish between cancer cells which were difficult to distinguish on the spectrum. Fig. 5a shows clear separation between the normal breast cells and breast cancer cells in the PCA score plot, where the first principle component explained 63.57% of the variance and the second component explained 20.89%. Additionally, while the breast cancer cells clustered near each other, the groups show clear separation from normal cells. Fig. 5b shows a PCA analysis on just the cancer cells, which clearly separates the two cell types, with the first principle component explaining 68.74% of the variance and the second component explaining 23.33%. The Raman spectrum regions that were responsible for the PCA discrimination were the phenylalanine, amide I, amide III, CH_2 deformation, CH_2 wagging/twisting, and S—S Bonding vibration peaks. Thus, components in the highly confined spectral region including the above chemical constitution alone occupy a large portion as a factor that differentiates the cell lines.

Table 1
The individual deviations and means in RGB intensity between applied cell lines.

Standard deviations (mean values)	MCF-10A	MDA-MB-231	MDA-MB-453
Red	28.1 (194.0)	10.3 (213.2)	8.1 (213.5)
Green	33.0 (209.8)	10.1 (215.2)	11.0 (217.8)
Blue	28.8 (215.9)	9.2 (214.3)	9.5 (217.2)

4. Conclusion

In summary, Raman spectra were acquired for the noninvasive cell line MFC-10A and invasive cancer cell lines MDA-MB-231, MDA-MB-453. The results showed major peaks in the regions for phenylalanine, amides I and III, CH_2 deformation, CH_2 wagging/twisting and S—S bonding vibration. These peaks may be useful as the main spectrum markers of cell invasiveness. Using those peaks as variables, PCA on spectral differences allowed for further discrimination between invasive and noninvasive cells. Although the breast cancer cells (MDA-MB-231 and MDA-MB-453) clustered close to each other when the PCA results were calculated for all three types of cells, each group was clearly differentiated when only the breast cancer cells were investigated. Additionally, the morphology dependence of Raman and RGB deviation from the transmitted optical signals was significant in distinguishing between the normal and cancer cell lines. Because Raman spectroscopy is a technique for detecting conformational changes, and if the optical interaction is measured with transmission of RGB in the radial direction of the cell, the characterization factor that distinguishes the normal and the cancer can be found locally. In the case of the normal breast cells (MCF-10A) in this study, the position-dependent reflected signal difference in the radial direction seemed to be due to the cell organelles. However, in malignant cells (MDA-MB-231 and MDA-MB-453), the conformational difference did not appear to be dependent on the intracellular location. Since there is little difference in the degree of transmission between the red, green, and blue spectral components across the

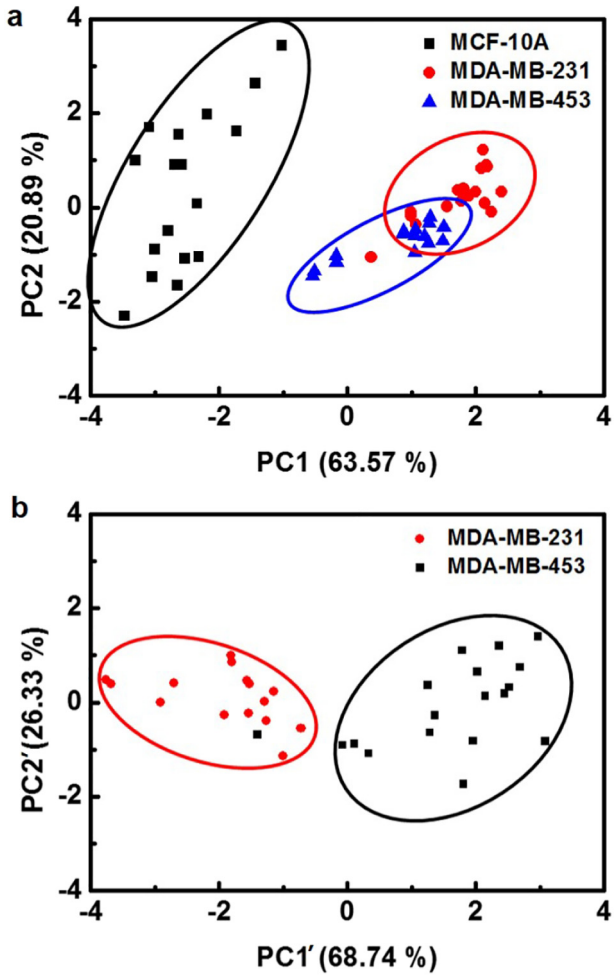

Fig. 5. PCA results for (a) MCF-10A, MDA-MB-231, and MDA-MB-453 and (b) MDA-MB-231 and MDA-MB-453.

cells, RGB and Raman characteristics offer promising data for understanding the mechanism of cancer cell development, diagnosis, and treatment. The study of the synchronization and local difference of Raman and RGB transmission in this cell unit suggests the methodology of label-free and non-destructive field study and has potential for application to other cell lines. When the results obtained in this study are implemented on tissue and tumor scale, this result should be a basic study for establishing clinical diagnostic criteria.

Disclosures

The authors have no relevant financial interests in this article and no potential conflicts of interest to disclose.

Acknowledgments

This work was supported by the Basic Science Research Program (2014R1A1A2057773, 2015K2A7A1035896) through the National Research Foundation of Korea (NRF) funded by the Ministry of Science & ICT (MSIT), and by the Ministry of Trade, Industry & Energy (MOTIE) under Industrial Technology Innovation Program (10052048, 10080726). This study was also supported by a grant (2015-641, 2015-646) from the Asan Institute for Life Sciences, Asan Medical Center, Seoul, Korea and by 'Software Convergence Technology Development Program', through the Ministry of Science, ICT and Future Planning (ITAS0177160110290001000200200).

References

[1] G. Christofori, Changing neighbours, changing behaviour: cell adhesion molecule-mediated signalling during tumour progression, EMBO J. 22 (2003) 2318–2323.
[2] J. Ferlay, H.R. Shin, F. Bray, D. Forman, C. Mathers, D.M. Parkin, Estimates of worldwide burden of cancer in 2008: GLOBOCAN 2008, Int. J. Cancer 127 (2010) 2893–2917.
[3] A. Mert, N. Kılıç, A. Akan, An improved hybrid feature reduction for increased breast cancer diagnostic performance, Biomed. Eng. Lett. 4 (2014) 285–291.
[4] H.J. Kwon, B. Shin, D. Gopaul, S. Fienberg, Strain ratio vs. modulus ratio for the diagnosis of breast cancer using elastography, Biomed. Eng. Lett. 4 (2014) 292–300.
[5] S. Rehman, Z. Movasaghi, A.T. Tucker, S.P. Joel, J.A. Darr, A.V. Ruban, I.U. Rehman, Raman spectroscopic analysis of breast cancer tissues: identifying differences between normal, invasive ductal carcinoma and ductal carcinoma in situ of the breast tissue, J. Raman Spectrosc. 38 (2007) 1345–1351.
[6] J.L. González-Solís, J. Rodríguez-López, J.C. Martínez-Espinosa, C. Frausto-Reyes, L.F. Jave-Suárez, A.C. Aguilar-Lemarroy, H. Vargas-Rodríguez, E. Martínez-Cano, Detection of cervical cancer analyzing blood samples with Raman spectroscopy and multivariate analysis, AIP Conference Proceedings, 1226, 2010, p. 91.
[7] B. Singh, R. Gautam, S. Kumar, B.N.V. Kumar, U. Nongthomba, D. Nandi, G. Mukherjee, V. Santosh, K. Somasundaram, S. Umapathy, Application of vibrational microspectroscopy to biology and medicine, Curr. Sci. India 102 (2012) 232–244.
[8] R. Gautam, A. Samuel, S. Sil, D. Chaturvedi, A. Dutta, F. Ariese, S. Umapathy, Raman and mid-infrared spectroscopic imaging: applications and advancements, Curr. Sci. India 108 (2015) 341–356.
[9] Y. Oshima, H. Shinzawa, T. Takenaka, C. Furihata, H. Sato, Discrimination analysis of human lung cancer cells associated with histological type and malignancy using Raman spectroscopy, J. Biomed. Opt. 15 (2010).
[10] X. Li, T. Yang, R. Wang, W. Wen, Surface Enhanced Raman Spectrum of Saliva for Detection of Lung Cancer, 2011 IEEE International Symposium on IT in Medicine and Education, Cuangzhou, 2011 688.
[11] A.S. Haka, K.E. Shafer-Peltier, M. Fitzmaurice, J. Crowe, R.R. Dasari, M.S. Feld, Diagnosing breast cancer by using Raman spectroscopy, Proc. Natl. Acad. Sci. U. S. A. 102 (2005) 12371–12376.
[12] A.S. Haka, Z. Volynskaya, J.A. Gardecki, J. Nazemi, R. Shenk, N. Wang, R.R. Dasari, M. Fitzmaurice, M.S. Feld, Diagnosing breast cancer using Raman spectroscopy: prospective analysis, J. Biomed. Opt. 14 (2009).
[13] A. Saha, I. Barman, N.C. Dingari, S. McGee, Z. Volynskaya, L.H. Galindo, W. Liu, D. Plecha, N. Klein, R.R. Dasari, M. Fitzmaurice, Raman spectroscopy: a real-time tool for identifying microcalcifications during stereotactic breast core needle biopsies, Biomed. Opt. Express 2 (2011) 2792–2803.
[14] H. Abramczyk, B. Brozek-Pluska, J. Surmacki, J. Jablonska-Gajewicz, R. Kordek, Raman 'optical biopsy' of human breast cancer, Prog. Biophys. Mol. Biol. 108 (2012) 74–81.
[15] L.E. Kamemoto, A.K. Misra, S.K. Sharma, M.T. Goodman, H. Luk, A.C. Dykes, T. Acosta, Near-infrared micro-Raman spectroscopy for in vitro detection of cervical cancer, Appl. Spectrosc. 64 (2010) 255–261.
[16] A. Mahadevan-Jansen, R. Richards-Kortum, Raman Spectroscopy for Cancer Detection: A Review, 6, IEEE Engineering in Medicine and Biology Society, 1997 2722.
[17] S.Y. Feng, J.J. Pan, Y.A. Wu, D. Lin, Y.P. Chen, G.Q. Xi, J.Q. Lin, R. Chen, Study on gastric cancer blood plasma based on surface-enhanced Raman spectroscopy combined with multivariate analysis, Sci. China Life Sci. 54 (2011) 828–834.
[18] T. Kawabata, H. Kikuchi, S. Okazaki, M. Yamamoto, Y. Hiramatsu, J.H. Yang, M. Baba, M. Ohta, K. Kamiya, T. Tanaka, H. Konno, Near-infrared multichannel Raman spectroscopy with a 1064 nm excitation wavelength for ex vivo diagnosis of gastric cancer, J. Surg. Res. 169 (2011) E137–E143.
[19] H. Sato, Y.S. Yamamoto, A. Maruyama, T. Katagiri, Y. Matsuura, Y. Ozaki, Raman study of brain functions in live mice and rats: a pilot study, Vib. Spectrosc. 50 (2009) 125–130.
[20] M. Kirsch, G. Schackert, R. Salzer, C. Krafft, Raman spectroscopic imaging for in vivo detection of cerebral brain metastases, Anal. Bioanal. Chem. 398 (2010) 1707–1713.
[21] M. Larraona-Puy, A. Ghita, A. Zoladek, W. Perkins, S. Varma, I.H. Leach, A.A. Koloydenko, H. Williams, I. Notingher, Development of Raman microspectroscopy for automated detection and imaging of basal cell carcinoma, J. Biomed. Opt. 14 (2009).
[22] M. Larraona-Puy, A. Ghita, A. Zoladek, W. Perkins, S. Varma, I.H. Leach, A.A. Koloydenko, H. Williams, I. Notingher, Discrimination between basal cell carcinoma and hair follicles in skin tissue sections by Raman micro-spectroscopy, J. Mol. Struct. 993 (2011) 57–61.
[23] Y. Li, Z.N. Wen, L.J. Li, M.L. Li, N. Gao, Y.Z. Guo, Research on the Raman spectral character and diagnostic value of squamous cell carcinoma of oral mucosa, J. Raman Spectrosc. 41 (2010) 142–147.
[24] U. Neugebauer, T. Bocklitz, J.H. Clement, C. Krafft, J. Popp, Towards detection and identification of circulating tumour cells using Raman spectroscopy, Analyst 135 (2010) 3178–3182.
[25] A. Shapiro, O.N. Gofrit, G. Pizov, J.K. Cohen, J. Maier, Raman molecular imaging: a novel spectroscopic technique for diagnosis of bladder cancer in urine specimens, Eur. Urol. 59 (2011) 106–112.
[26] H. Abramczyk, B. Brozek-Pluska, J. Surmacki, J. Jablonska, R. Kordek, The label-free Raman imaging of human breast cancer, J. Mol. Liq. 164 (2011) 123–131.
[27] R. McQueenie, R. Stevenson, R. Benson, N. MacRitchie, I. McInnes, P. Maffia, K. Faulds, D. Graham, J. Brewer, P. Garside, Detection of inflammation in vivo by surface-enhanced Raman scattering provides higher sensitivity than conventional fluorescence imaging, Anal. Chem. 84 (2012) 5968–5975.
[28] M. Marro, A. Taubes, A. Abernathy, S. Balint, B. Moreno, B. Sanchez-Dalmau, E.H. Martinez-Lapiscina, I. Amat-Roldan, D. Petrov, P. Villoslada, Dynamic molecular

monitoring of retina inflammation by in vivo Raman spectroscopy coupled with multivariate analysis, J. Biophotonics 7 (2014) 724–734.
[29] Y.J. Lee, G.J. Lee, S.W. Kang, Y. Cheong, H.K. Park, Label-free and quantitative evaluation of cytotoxicity based on surface nanostructure and biophysical property of cells utilizing AFM, Micron 49 (2013) 54–59.
[30] K. Haase, A.E. Pelling, Investigating cell mechanics with atomic force microscopy, J. R. Soc. Interface 12 (2015).
[31] G. Bao, S. Suresh, Cell and molecular mechanics of biological materials, Nat. Mater. 2 (2003) 715–725.
[32] Q.S. Li, G.Y.H. Lee, C.N. Ong, C.T. Lim, AFM indentation study of breast cancer cells, Biochem. Biophys. Res. Commun. 374 (2008) 609–613.
[33] A. Calzado-Martin, M. Encinar, J. Tamayo, M. Calleja, A.S. Paulo, Effect of actin organization on the stiffness of living breast cancer cells revealed by peak-force modulation atomic force microscopy, ACS Nano 10 (2016) 3365–3374.